Journal of Marine Science and Technology

Volume 26 | Issue 5 Article 7

PERFORMANCE ANALYSIS OF AN ACTIVE HEAVE COMPENSATION SYSTEM ON AN OFFSHORE SUPPLY VESSEL USING THE HARDWARE-IN-THE-LOOP SIMULATION

Luman Zhao
Graduate Student, Department of Naval Architecture and Ocean Engineering, Seoul National University, Republic of Korea

Myung-Il Roh
Professor, Department of Naval Architecture and Ocean Engineering, Research Institute of Marine Systems Engineering, Seoul National University, Republic of Korea

Recommended Citation

Zhao, Luman and Roh, Myung-Il (2018) "PERFORMANCE ANALYSIS OF AN ACTIVE HEAVE COMPENSATION SYSTEM ON AN OFFSHORE SUPPLY VESSEL USING THE HARDWARE-IN-THE-LOOP SIMULATION," *Journal of Marine Science and Technology*: Vol. 26: Iss. 5, Article 7.
DOI: 10.6119/JMST.201810_26(5).0007
Available at: https://jmstt.ntou.edu.tw/journal/vol26/iss5/7

Journal of Marine Science and Technology, Vol. 26, No. 5, pp. 678-691 (2018)
DOI: 10.6119/JMST.201810_26(5).0007

PERFORMANCE ANALYSIS OF AN ACTIVE HEAVE COMPENSATION SYSTEM ON AN OFFSHORE SUPPLY VESSEL USING THE HARDWARE-IN-THE-LOOP SIMULATION

Luman Zhao[1], Myung-Il Roh[2], and Seung-Ho Ham[3]

Key words: active heave compensation system, hardware-in-the-loop simulation, multibody system, integrated simulation interface, offshore supply vessel.

ABSTRACT

The active heave compensation (AHC) system on an offshore supply vessel (OSV) plays a pivotal role in offshore installation operations by minimizing the heave motion of suspended subsea equipment, regardless of the OSV motion. In order to successfully perform its function, the AHC system should have a suitable control algorithm, and its performance must be evaluated in advance of operation. Performance analysis of the AHC system requires complicated testing procedures, and a great deal of associated equipment. In particular, such analysis is often very costly and time-consuming, and realistic conditions are typically impossible to establish in a testing environment. To solve this problem, the Hardware-In-the-Loop Simulation (HILS) concept can be used as an effective method to test an AHC system prior to its final installation. In this study, we have constructed the HILS environment for an AHC system for an OSV, and conducted a performance analysis of the AHC system. To do so, a virtual model of the OSV was first created from a multibody system that can represent realistic motion in waves. Then, a controller of the AHC system with a control algorithm for heave compensation was implemented on real hardware. Next, an integrated simulation interface was implemented to efficiently connect the virtual model and the controller, and a visualization model was developed to verify simulation results by immersive and realistic views. Finally, a performance analysis of the AHC system was conducted within the proposed HILS environment. A numerical example is a deadweight 3,500 ton OSV to install a subsea manifold in regular and irregular waves. A comparative study between uncontrolled and controlled results of the AHC system was further performed. As a result, the performance of the AHC system could be evaluated effectively within the HILS environment.

I. INTRODUCTION

Generally, an Offshore Supply Vessel (OSV) provides support services to offshore oil and gas field development, such as offshore drilling, pipe laying, and oil producing assets (production platforms and Floating Production Storage and Offloading (FPSO)) utilized in Exploration & Production (E & P) activities. One of the main activities of the OSV is to install various items of subsea equipment, such as subsea manifolds, on the seabed. For this, the OSV has a crane mounted on its deck. Fig. 1 shows an example of the installation of a subsea manifold using the OSV crane mounted on its deck.

Meanwhile, waves induce motion of the OSV, which induces similar effects on the subsea equipment suspended by the OSV crane. Hence, special equipment called an Active Heave Compensation (AHC) system is also included in the OSV crane, as shown in Fig. 1. The AHC system is used to reduce the motion of the suspended subsea equipment by controlling the length of the associated wire rope. Fig. 2 describes the control mechanism of the AHC system.

At first, a Motion Reference Unit measures the position and orientation of the OSV. This information is transferred to an AHC controller, in order to control the motor. The AHC controller calculates the depth of the subsea equipment according to the position and orientation of the OSV and the OSV crane. If the depth of the subsea equipment is less than the target depth, the AHC controller sends a lowering signal to extend the length of the wire rope. Otherwise, the AHC controller sends a hoisting signal to shorten the length of the wire rope.

Since the AHC controller is most responsible for the success-

Paper submitted 11/16/17; revised 03/20/18; accepted 08/16/18. Author for correspondence: Myung-Il Roh (e-mail: miroh@snu.ac.kr).
[1] Graduate Student, Department of Naval Architecture and Ocean Engineering, Seoul National University, Republic of Korea.
[2] Professor, Department of Naval Architecture and Ocean Engineering, Research Institute of Marine Systems Engineering, Seoul National University, Republic of Korea.
[3] Post Doc., Research Institute of Marine Systems Engineering, Seoul National University, Republic of Korea.

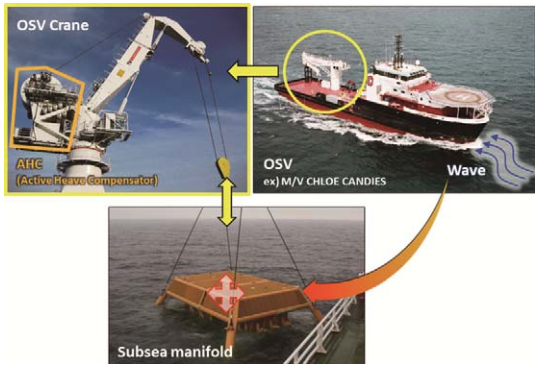

Fig. 1. An example of the use of the OSV to install a subsea manifold.

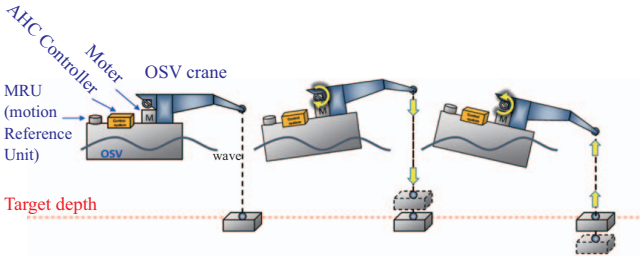

Fig. 2. The mechanism of the AHC system.

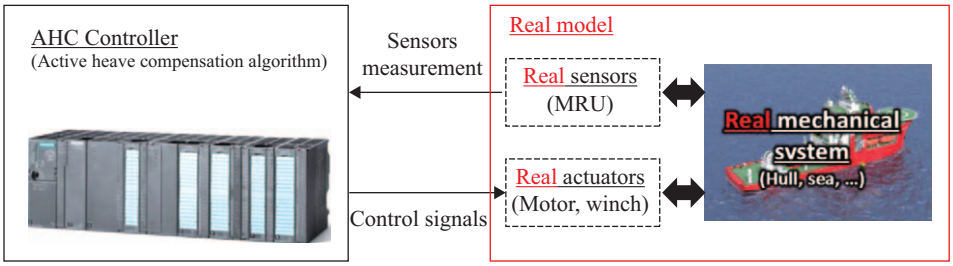

Fig. 3. Test environment of the AHC controller by using a real model.

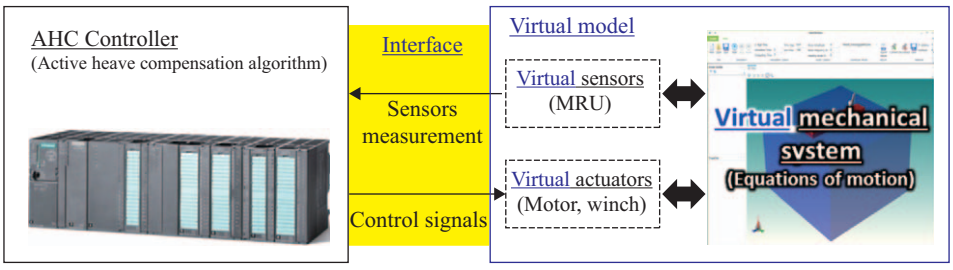

Fig. 4. Test environment of the AHC controller by using the virtual model.

ful operation of the crane, the AHC controller must have a suitable control algorithm, and its performance should be evaluated in advance. Performance analysis of the AHC system requires a complicated test procedure, and a great deal of equipment. Fig. 3 shows the test environment of the AHC controller using the real model.

This real model requires real sensors, actuators, and mechanical systems to generate true sensor measurements, and receive control signals. This test environment is very costly, and it is nearly impossible to guarantee completely safe conditions for testing. Moreover, it is time consuming to test while at sea, and particularly difficult to identify bugs before testing. Therefore, to overcome these defects, the idea of replacing real sensors, actuators, and mechanical system by virtual ones is introduced, as shown in Fig. 4.

This testing environment is called Hardware-In-the-Loop

Table 1. Related studies of HILS for AHC and comparison with this study.

Studies	Controller	Virtual model		Interface	Visualization model	Applications	
		Dynamics	Environmental condition			Maintaining the depth of the subsea equipment	Lowering the subsea equipment
Hu et al. (2009)	PCI eXtensions for Instrumentation (PXI)	Matlab	×	LabVIEW	×	×	×
Muraspahic et al. (2012)	Siemens controller	Simulation X	×	Simulink	×	○	×
Aarseth et al. (2014)	Bachmann M1 controller	20-sim	○	Ethernet	○	×	×
This study	Siemens controller	In-house Code	○	HLA/RTI and OPC	○	○	○

Simulation (HILS), and represents a technique that is used in the development and testing of a complex control system interacting with a virtual model. This virtual model is included in the testing and development by adding mathematical representation of all related dynamic systems. The test in the HILS environment is less expensive than the real test, because all parts, with the exception of the controller, can be replaced by software. It can also generate any environmental conditions, takes less time for testing, and allows bugs to be found in advance.

Four components for HILS of the AHC system are proposed in this study. Fig. 4 shows that basically three components, such as a virtual model, controller, and interface, are required. The virtual model of the OSV can consist of a multibody system, which can represent realistic motion in waves. The controller of the AHC system having a control algorithm for heave compensation is implemented on real hardware. An integrated simulation interface is adopted to transfer signals efficiently between the virtual model and the controller through the network. In addition to these three components, the visualization model based on Virtual Reality (VR) is also integrated, to check simulation results through immersive and realistic views.

II. RELATED STUDIES

The general concept of HILS is comprehensively summarized in Schlager et al. (2006) and Popovici et al. (2013). HILS technology has been widely used in the defense and aerospace industries as early as the 1950s. At that time, in spite of the high cost of HILS technology, these industries benefitted greatly from its safety. During the past decade, the advancement of computer technology has led to the adoption of HILS to automotive systems in the 1990s (Nabi et al., 2004). Isermann et al. (1999) performed an efficient real-time HILS for Electronic Control Unit design and verification. Similar work has recently been done by Fathy et al. (2006), in providing an overview of HILS for an engine system and its prospects in the automotive area.

For the offshore industry, ships and offshore structures are equipped with advanced control systems for Dynamic Positioning and Power Management. Unlike the mass production of the automation industry, the controller is unique for each vessel or offshore structure. In this context, HILS seems indispensable in this field. Several works proposed by Pedersen et al. (2013) and Kaliappan et al. (2012) were dedicated to providing experience to implement HILS for DP and PM systems.

Furthermore, HILS for the AHC system is an important field. Hu et al. (2009) performed HILS with mathematical models and physical testing of an AHC system on a pipeline lifting mining system. The simulation is based on a controller (PXI) from LabVIEW. Another common tool (Simulink) is also widely used as a connection interface between controller and virtual model. This was implemented in Muraspahic et al. (2012). The virtual model was modeled by commercial software (Simulation X), without considering environmental conditions. The Siemens PLC (Programmable Logic Controller) was utilized as a controller regulating the virtual model. The visualization model only displayed a simple winch model. An attempt to build the virtual model based on the Bond Graph method was presented by Aarseth et al. (2014). The virtual model was described as the energy flow by using 20-sim. Even though the software can display 3D-animation for development, there are some limitations in terms of the visualization model based on VR. Table 1 summarizes the related studies mentioned above to compare with this study.

III. COMPONENTS FOR THE HILS ENVIRONMENT OF THE AHC SYSTEM

This section presents definitions and the theoretical background of four components, such as a virtual model, controller, visualization model, and interface for HILS of the AHC system in detail. The virtual model replaces the real OSV by solving equations of motion of the OSV, the OSV crane, and the subsea equipment. The virtual model is composed of a virtual mechanical system, virtual sensors, and virtual actuators.

1. Virtual Mechanical System

To represent the virtual mechanical system, the equations of motion of the OSV, the OSV crane, and the subsea equipment, including wave loads as an external force, must be formulated. They should be solved simultaneously, because these bodies are closely related to each other by joints or wire ropes, as shown in Fig. 5. Hence, this is referred to as a multibody system (Cha

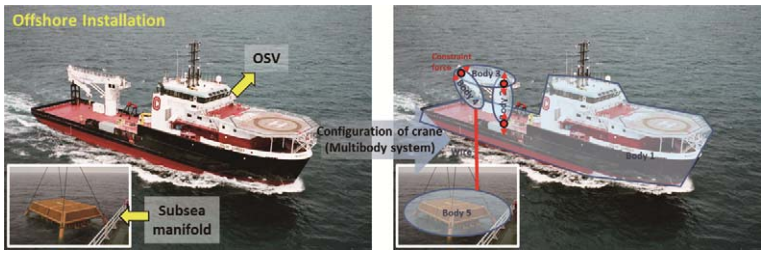

Fig. 5. Multibody system of OSV, OSV crane, and subsea manifold.

et al., 2010).

It is very difficult to apply a Newton-Euler equation directly to the multibody system in the case of existing constraints and constraint forces. Therefore, we change the form of the Newton-Euler equation to the formulation for multibody system dynamics. Here, we choose the discrete Euler-Lagrange equation (Ham et al., 2015b). A variational principle is introduced in Fowles and Cassiday (2005). To compute a discrete trajectory of a body, the concept of virtual displacement and virtual work can be considered. According to Hamiltons's principle, which addresses the expenditure of energy in the system during motion, the action integral J can be defined as:

$$J = \int_{t_1}^{t_2} L dt = \int_{t_1}^{t_2} (T - V) dt \tag{1}$$

where, T and V are the kinetic and potential energy of the particle, respectively, and L is called the Lagrangian. During a time interval from t_1 to t_2, the actual motion minimizes the above integral. This can be expressed mathematically as:

$$\delta J = \delta \int_{t_1}^{t_2} (T - V) dt = \delta \int_{t_1}^{t_2} L dt \tag{2}$$

From Eq. (2), we can deduce the Euler-Lagrange equation, which is known to be:

$$\frac{d}{dt}\left(\frac{\partial L}{\partial \dot{\mathbf{q}}}\right) - \frac{\partial L}{\partial \mathbf{q}} = 0 \tag{3}$$

A discrete Euler-Lagrange equation is utilized in Lew (2003), and Marsden and West (2001). The action integral of the Lagrangian of Eq. (1) can be represented by the sum of an infinitesimal area with time divided into small time steps h. Approximating each infinitesimal area as a rectangular shape, and the velocity $\dot{\mathbf{q}}_k$ as $\frac{\mathbf{q}_{k+1} - \mathbf{q}_k}{h}$, the discrete action integral of the Lagrangian J_d can be expressed by:

$$J_d = \sum_{k=0}^{N-1} L_d (\mathbf{q}_k, \mathbf{q}_{k+1}, h) \tag{4}$$

where, h is the time step, and $\mathbf{q}_k$ is the position of the particle at time $t_1 + kh$. According to the variational principle, the particle moves along the trajectory where δJ is zero. Thus, the formula can be expressed as:

$$\begin{aligned} \delta J_d &= \sum_{k=0}^{N-1} \delta L_d (\mathbf{q}_k, \mathbf{q}_{k+1}, h) \\ &= \sum_{k=1}^{N-1} \left[D_2 L_d (\mathbf{q}_{k-1}, \mathbf{q}_k, h) + D_1 L_d (\mathbf{q}_k, \mathbf{q}_{k+1}, h) \right] \delta \mathbf{q}_k = 0 \end{aligned} \tag{5}$$

where, D_i is the partial differential operator, which means the partial differentiation by the i^{th} variable. As a result, Eq. (5) can be expressed in the form of a discrete Euler-Lagrange equation:

$$D_2 L_d (\mathbf{q}_{k-1}, \mathbf{q}_k, h) + D_1 L_d (\mathbf{q}_k, \mathbf{q}_{k+1}, h) = 0 \tag{6}$$

Considering the system with constraints $\overline{L} = L + \sum_{j=1}^{m} \lambda_j g_j (\mathbf{q})$ and external forces, the discrete Euler-Lagrange equations for the system can be obtained, namely:

$$\begin{aligned} &D_2 L_d (\mathbf{q}_{k-1}, \mathbf{q}_k, h) + D_1 L_d (\mathbf{q}_k, \mathbf{q}_{k+1}, h) + \sum_{j=1}^{m} h \lambda_{jk} \left(\frac{\partial g_j}{\partial \mathbf{q}_k} \right) \\ &\quad + f_d^{\alpha+} (\mathbf{q}_{k-1}, \mathbf{q}_k) + f_d^{\alpha-} (\mathbf{q}_k, \mathbf{q}_{k+1}) = 0 \end{aligned} \tag{7}$$

According to a Taylor series expansion, the constraints can be expressed by:

$$\sum_{j=1}^{m} g_j (\mathbf{q}_{k+1}) = \sum_{j=1}^{m} \left[g_j (\mathbf{q}_k) + \frac{\partial g_j}{\partial \mathbf{q}_k} (\mathbf{q}_{k+1} - \mathbf{q}_k) \right] = 0 \tag{8}$$

From Eq. (7) and the constraints (Eq. (8)), we can derive the discrete Euler-Lagrange equations in matrix form:

$$\begin{aligned} &\begin{bmatrix} \mathbf{M} & -\mathbf{G}_k^T \\ \mathbf{G}_k & 0 \end{bmatrix} \begin{bmatrix} \mathbf{q}_{k+1} \\ h^2 \boldsymbol{\lambda}_k \end{bmatrix} \\ &= \begin{bmatrix} \mathbf{M} (2\mathbf{q}_k - \mathbf{q}_{k-1}) - h^2 \dfrac{\partial V}{\partial \mathbf{q}_k} + h^2 \mathbf{f} \left(q_k, \dfrac{q_k - q_{k-1}}{h} \right) \\ -\mathbf{g} (\mathbf{q}_k) + \mathbf{G}_k \mathbf{q}_k \end{bmatrix} \end{aligned} \tag{9}$$

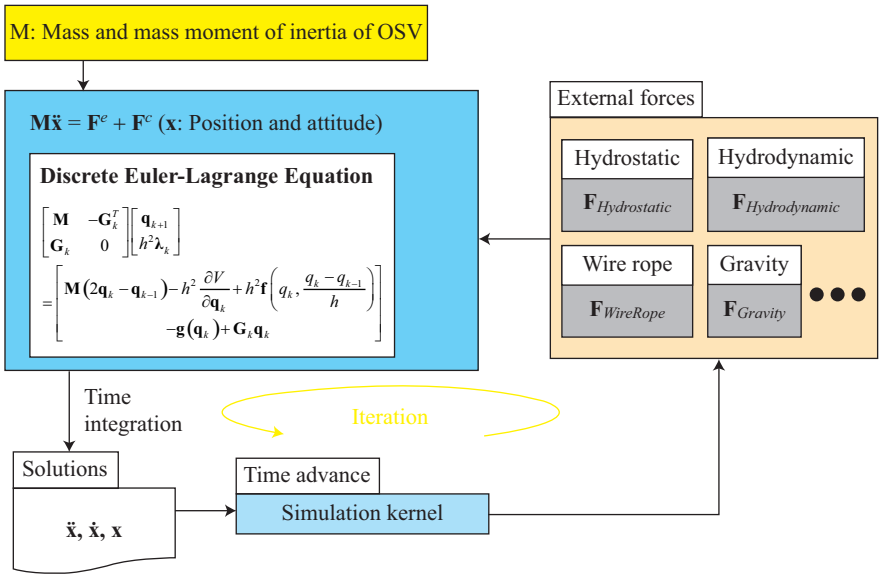

Fig. 6. The numerical analysis procedure of the OSV crane system.

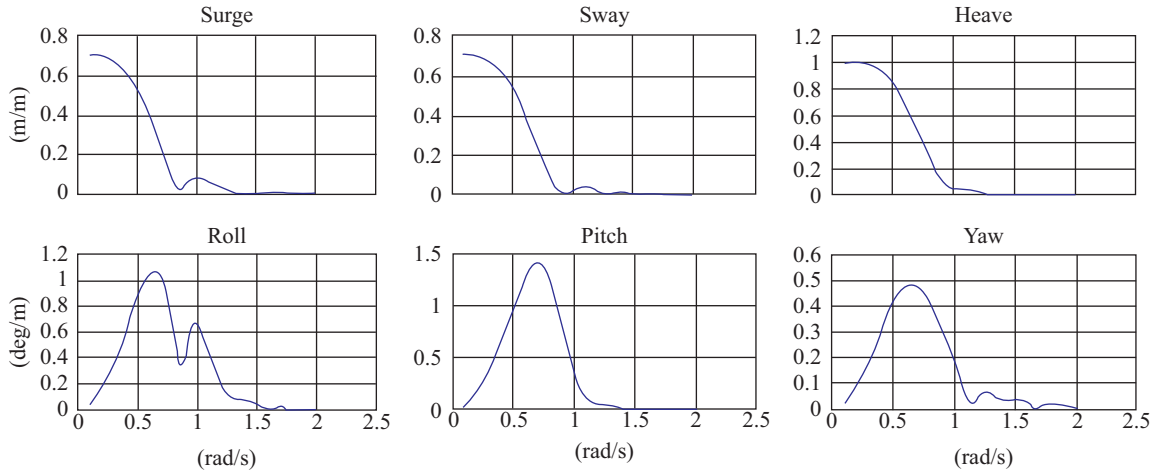

Fig. 7. Motion RAOs of the OSV for a heading angle of 45 degree.

Now, the motion of the OSV, including the OSV crane and the subsea equipment, can be calculated according to the procedure in Fig. 6, considering wave loads as an external force.

When the simulation starts, the equations of motion of the OSV can be solved to find its acceleration. Then the velocity and position are successively calculated by time integration (Ham et al., 2015b; Hong et al., 2015). Based on the obtained velocity and position, the external forces, including the radiation, diffraction, Froude-Krylov, and restoring forces, are updated for the next time step.

The hydrodynamic force can be divided into two parts: the wave exciting force, which is exerted by the incident wave; and the radiation force from the wave, generated by the motion of the floater itself. This is expressed as:

$$\mathbf{F}_{hydrodynamic} = \mathbf{F}_{exciting} + \mathbf{F}_{radiation} \tag{10}$$

$\mathbf{F}_{exciting}$ is calculated by multiplying the force Response Amplitude Operator (RAO) with the sinusoidal function at a given frequency. The force RAO can be obtained from a commercial solver, such as Wave Analysis by Diffraction and Morison (WADAM) by DNV (2002). The Cummins equation (Cummins, 1962) can be used to calculate $\mathbf{F}_{radiation}$, which considers the impulse response of the floater in the time domain. The frequency-dependent added mass coefficient $a_{ij}(\omega)$ and the frequency-dependent damping coefficient $b_{ij}(\omega)$ at a given frequency ω can also be obtained from the commercial solver. Using the frequency-dependent coefficients $a_{ij}(\omega)$ and $b_{ij}(\omega)$, the added mass $\mathbf{A}$ and retardation function $\mathbf{B}(\tau)$ can be determined. The infinite added mass $\mathbf{A}_{\infty}$, which is a constant matrix, is often used, rather than calculating the above integral.

In the case of a regular wave, only one wave frequency should be chosen according to a single wave amplitude (a). The motions

Principal Dimensions

Length O.A.	85.25 (m)
Length waterline	81.7 (m)
Breadth molded	18 (m)
Depth molded	7.4 (m)
Design/Scantling draft	5.0/6.0 (m)
Deadweight	3,500 (ton)

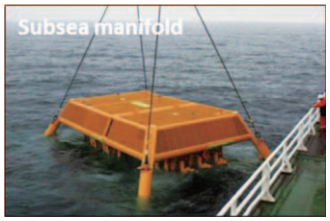

Principal Dimensions

Length	20.3 (m)
Breadth	15.0 (m)
Height	6.1 (m)
weight	175 (ton)

Fig. 8. Principal dimensions of the target OSV and subsea manifold.

RAOs of OSV can be obtained from a commercial solver like WADAM. Fig. 7 shows an example of the motion RAOs for a heading angle of 45 degree.

However, in the case of an irregular wave, there are a number of N wave frequencies and amplitudes, according to the given wave spectrum.

$$\mathbf{F}_{exciting} = \sum_{m=1}^{N} a_m \cdot \mathbf{F}(\omega_m)\cos(\omega_m t + \varepsilon_m) \tag{11}$$

Based on the exciting force theory proposed by Journée and Massie (2001), Eq. (11) is the linear superposition, which can be calculated in irregular wave. Since the first order wave force is a linear phenomenon, time history of the first order wave loads in a certain sea state can be obtained from frequency domain calculations by using the frequency characteristics of the first order wave loads, and the wave spectrum, by using the superposition principle. So that the time history of the first order wave loads becomes Eq. (11) with chosen phase shifts.

Fig. 8 shows the shape and principal dimensions of the target OSV (M/V CHLOE CANDIES). The principal dimensions of the OSV are 85.25 m in length, 18 m in breadth, and 7.4 m in depth, while its deadweight is 3,500 tons. The principal dimensions of the subsea manifold are 20.3 m in length, 15 m in breadth, and 6.1 m in depth. Its weight is 175 tons.

Fig. 9 shows that the OSV and the crane are composed of several rigid bodies.

The pedestal of the crane (Body 2) is attached to the deck of the OSV barge (Body 1). The knuckle boom has upper and lower arms, which are depicted as Body 3 and Body 4. Those rigid bodies are connected by revolute joints, which can allow only one rotational motion perpendicular to the joint axis. The subsea manifold (Body 5) is suspended by a single wire rope from the tip of the upper arm. As an initial condition, the wire length is 197.1 m below the sea surface. Because those bodies are connected by joints and the wire rope, the motions are closely related to the others. The OSV barge is the only part upon which

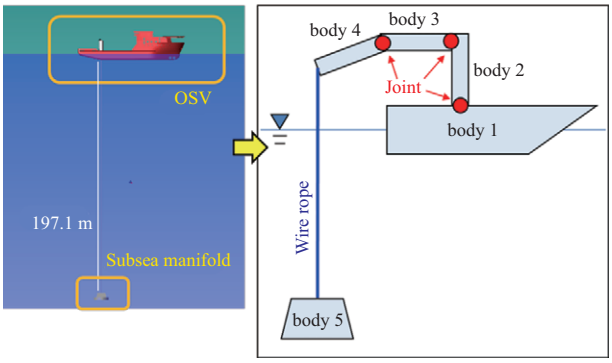

Fig. 9. Rigid body models of the OSV and the crane.

the hydrodynamic force is exerted.

In this study, the wire rope is modeled by the incompressible spring, which adds the force only when it is extended. It is calculated as follows:

$$\mathbf{F}_{Wirerope} = k \cdot (x - x_0), \ (only\ if\ x > x_0) \tag{12}$$

where, k is the spring constant, which measures how stiff and strong the spring is; and $x - x_0$ is the distance when the spring is stretched from its equilibrium position.

The added mass of the subsea manifold, which is immersed inside the seawater, should be considered. Because the vertical motion of the manifold is dominant during the operation, we can estimate the added mass roughly by the rectangular plate (DNV, 2011). The vertical added mass of the subsea manifold is obtained from the following equation:

$$\begin{aligned} M_{added,virtical} &= \rho C_A V_R \\ &= 1.025 \times 0.66 \times (20.3 \times 15) \\ &= 206\ [ton] \end{aligned} \tag{13}$$

where, C_A is the added mass coefficient, and V_R is the reference volume. It is interpolated by the ratio of the length and breadth of the subsea manifold (DNV, 2011).

2. Virtual Sensor and Actuator

Sensor measurements from the real sensor are used to control the real actuator. Fig. 10 shows the procedure to control the length of the wire rope with the real sensors and actuator.

An MRU is a motion reference device that is capable of measuring pitch, roll, heave, and heading to a high degree of accuracy, and is suitable for any maritime operation. In the real OSV, the measurements are transferred to the controller. The controller sends voltage to regulate the rotating speed of the motor. Finally, the torque causes the winch to rotate, and controls the wire rope length. In this study, the real sensor and actuator should be replaced by a virtual sensor and actuator. Fig. 11 describes how to implement a virtual sensor and actuator.

At first, the virtual sensor is implemented by simply receiving

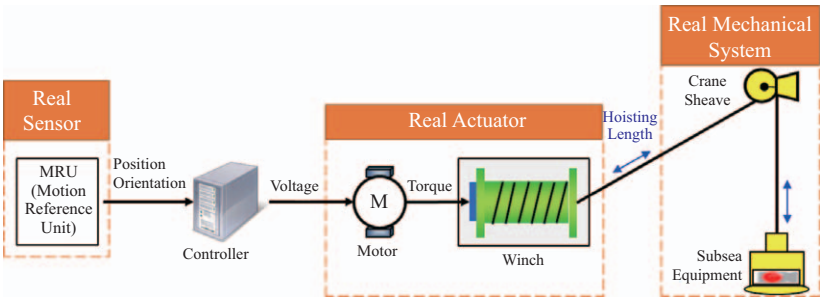

Fig. 10. The procedure to control the wire rope length with the real sensors and actuator.

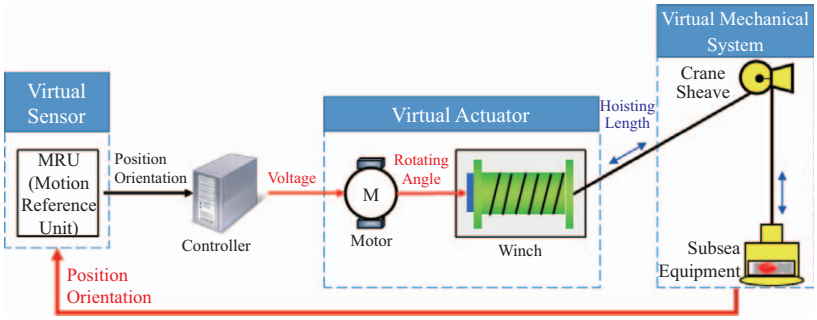

Fig. 11. Implementation of the virtual sensor and actuator.

the motion data calculated from the virtual mechanical system. The virtual actuator calculates the rotating angle of the winch by integrating the rotating speed from the controller. Finally, the winch changes the length of the wire rope according to the rotating angle.

The virtual actuator we chose in this study comprised servo-valve and hydraulic motor. The servo-valve is a device that uses mechanical motion to deliver a measured amount of fluid power to the hydraulic motor. The mechanical motion is induced by the electrical current that changes in proportion to the displacement of the spool attached on the valve (Eq. (14)).

$$x_v \approx \frac{k_t i}{k(r+b)} \tag{14}$$

where, x_v is the spool position changed by the current input i. As a result, the movement of the spool can change the load flow into the two chambers of the hydraulic motor. The load flow q_L represents the average of the flows in the lines connected between the servo-valve and the hydraulic motor, which can be linearized as follows:

$$q_L = K_q x_v - K_c p_L \tag{15}$$

where,

$$K_q = C_d b \sqrt{\frac{1}{\rho}(p_s - \mathrm{sgn}(x_v) p_L)}$$
$$K_c = \frac{C_d b x_v \sqrt{1/\rho}(p_s - \mathrm{sgn}(x_v) p_L)}{2(p_s - \mathrm{sgn}(x_v) p_L)} \tag{16}$$

In addition, the dynamic model of the hydraulic motor can be derived based on the following equations:

$$\frac{V_t}{4\beta}\dot{p}_L = -C_{tm} p_L - D_m \omega_m + q_L$$
$$J_t \dot{\omega}_m = -B_m \omega_m + D_m p_L - T_L \tag{17}$$

Consequently, the speed of the motor shaft can be controlled by the electrical current.

By combining the above Eq. (14) with Eq. (17), the linear dynamic model of the servo valve controlled hydraulic motor can be formulated by inserting the linearized valve characteristics into the model (Merritt, 1967).

$$\begin{bmatrix} \frac{V_t}{4\beta} & 0 & 0 \\ 0 & J_t & 0 \\ 0 & 0 & 1 \end{bmatrix} \begin{bmatrix} \dot{p}_L \\ \dot{\omega}_m \\ \dot{\theta}_m \end{bmatrix} = \begin{bmatrix} -K_{cei} & -D_m & 0 \\ D_m & -B_m & 0 \\ 0 & 1 & 0 \end{bmatrix} \begin{bmatrix} p_L \\ \omega_m \\ \theta_m \end{bmatrix} + \begin{bmatrix} K_p \\ 0 \\ 0 \end{bmatrix} i + \begin{bmatrix} 0 \\ -T_L \\ 0 \end{bmatrix} \tag{18}$$

where, V_t and D_m are the total volume and displacement of the hydraulic motor chambers, respectively; T_L is the load torque on the hydraulic motor, J_t is the moment of inertia of the hydraulic motor, and θ_m denotes the motor shaft angle; and K_{cei} is the leakage coefficient of the hydraulic motor and servo-valve, B_m is the viscous friction coefficient, and β is the bulk modulus. These parameters listed above represent the valve characteristics.

3. Controller of the AHC System

The controller of the AHC system is implemented on real

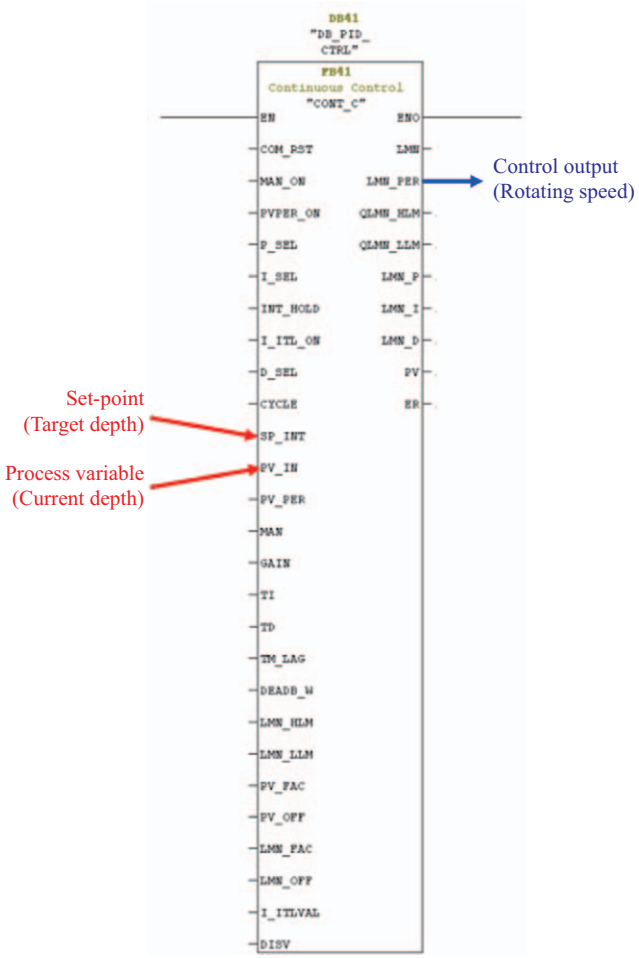

Fig. 12. Programmable PID control function block (FB41) and its input and output ports.

hardware. We used a Siemens PLC, which is well adapted to a range of automation tasks, and is widely used in motion control and positioning control around the world. The processor in the PLC plays an important role that manages the inputs and the outputs. It will receive the signal input from sensors, process the input signal, and then send the control signals to the actuators. The control algorithm in the controller is programmed by using the specific software on a PC.

In order to design the control algorithm, Proportional-Integral-Derivative (PID) control, which is commonly used as a control loop feedback mechanism, is adopted. For this, a programmable PID control function block (FB41) can be used. It is developed in a programming environment (SIMATIC STEP 7), which is a specific programming tool, and then downloaded to the controller. Signals in FB41 for the controller are specified by set-point, process variable, and controller output, which are set to the ports in the input and output modules respectively. Fig. 12 shows the programmable PID control function block (FB41) and its input and output ports.

A mathematical description of the PID controller is shown in the following equation:

$$u(t) = K_P[e(t) + \frac{1}{T_I}\int_0^t e(\tau)d\tau + T_D\frac{de(t)}{dt}] \quad (19)$$

where, $u(t)$ is the control signal, and $e(t)$ is the error signal. The control algorithm of the AHC system is used to minimize the heave motion of the subsea equipment. Therefore, the set-point (SP_INT) in the control algorithm is the target depth of the subsea equipment. The difference between the process variable (PV_IN) and the set point (SP_INT) is the error signal $e(t)$; Kp (GAIN) is the proportional gain, T_I (TI) and T_D (TD) are the integral and derivative time constants, respectively; and $K_I = K_P/T_I$ and $K_D = K_P T_D$ are the integral gain and derivative gain respectively. Thus these PID gain values (GAIN, TI, and TD) that are shown in Fig. 12 can be tuned through simulation to achieve the desired AHC performance of the system. In this study, the position of the equipment, which is calculated in real time, is sent to the controller, and is regarded as the process variable input. The control algorithm continuously calculates the difference between the set-point and the current depth of the subsea equipment, to minimize the difference over time, by adjusting the rotating speed of the motor. To accomplish this, it transmits to the virtual actuator, and the process repeats, until the subsea manifold can maintain the target depth.

4. Visualization Model

The visualization model is not necessary for HILS. However, it can be used to help users check the simulation results through immersive and realistic views, and can be used for training purposes. In this study we used Unity, which has many advantages, such as low price, good performance, and various visual effects. In particular, the environment around the OSV, including a sky with clouds and an ocean with reflection properties, and realistic waves, was modelled for faithful visualization. The visualization model changes the position and orientation based on the results from the virtual mechanical system in real time. Fig. 13 shows the visualization model of the OSV and the subsea manifold.

5. Integrated Simulation Interface

The three-component system, consisting of the virtual model, the controller, and the visualization model, is difficult to integrate, as each piece possesses its own development purposes and environment. Therefore, a simulation interface for integrating these different technologies efficiently and conveniently within a single system is proposed (Ham et al., 2015a; Ham et al., 2015c). This is composed of integrated simulation middleware and an adapter. The integrated simulation middleware connects all the simulation components, rather than merely transferring data amongst them. It also synchronizes the overall simulation time, even though it is not housed within the same computer. The adapter is plugged into each simulation component to connect it to the middleware. Fig. 14 shows the integrated simulation middleware and adapters for HILS of the AHC system.

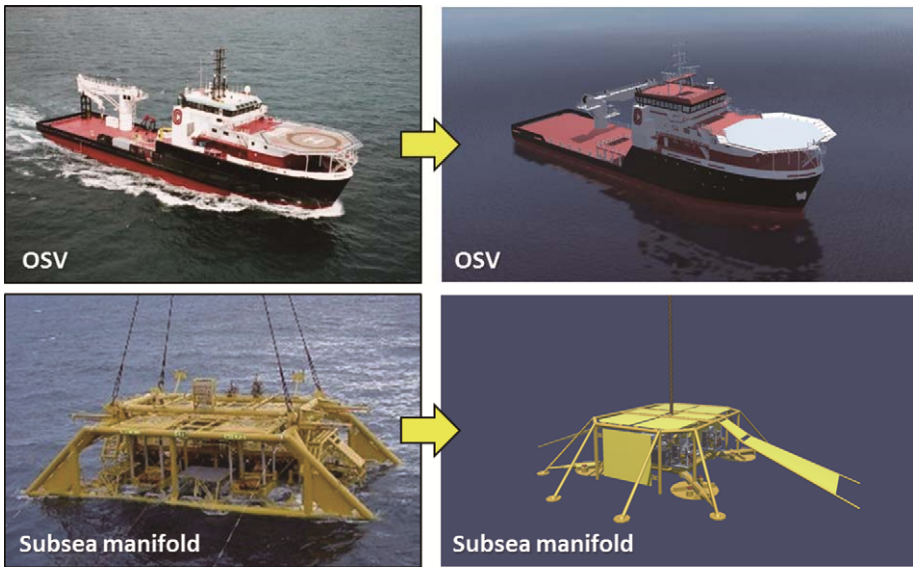

Fig. 13. Visualization model of the OSV and the subsea manifold.

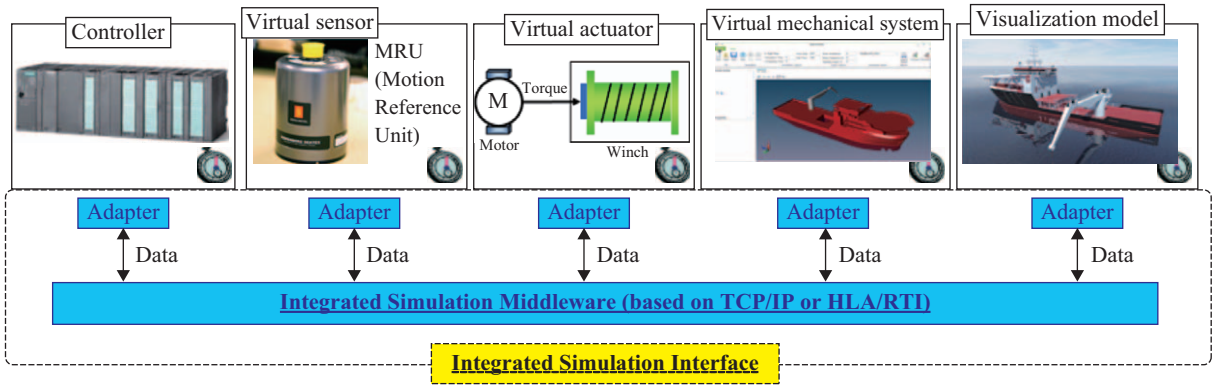

Fig. 14. Integrated simulation middleware and adapters for HILS of the AHC system.

The sensor measurement from the real sensor is transferred to the input module of the controller. Control signals are transferred from the output module to the real actuator. However, the controller is implemented on real hardware, whereas the others are software executed on the PC. Therefore, the controller should provide a kind of protocol to connect with a PC, and share the values through the network. Fig. 15 shows the method used to connect the controller to the virtual model.

To establish the interface between the AHC controller and the middleware, the OLE for Process Control (OPC), which is a standard based on the OPC server/client model, is used in this study. All variables, including the process variable and controller output, can be transmitted through the OPC server to the OPC client (OPC Foundation, 2016).

Fig. 16 shows the procedure for HILS of the AHC system with an integrated simulation interface.

First, the positions and orientation from the virtual mechanical system obtained by solving the equations of motion are transferred to the virtual sensor and visualization model (Fig. 16-❶). Next, the same data from the virtual sensor are also sent to the controller (Fig. 16-❷). The virtual actuator receives the rotating speed from the controller to maintain the subsea manifold at the target depth (Fig. 16-❸). Finally, the virtual actuator sends hoisting length information to the virtual mechanical system, to lengthen or shorten the wire rope length. This procedure is repeated at every time step.

6. Implementation of the HILS Environment of the AHC System

Fig. 17 shows the implementation of the HILS environment of the AHC system.

Two visualization models display the outside view of the OSV and Remotely Operated Vehicle (ROV) view of the subsea manifold. One PC is in charge of the virtual model including the virtual actuator, virtual sensor, and virtual mechanical system. The control algorithm is downloaded to the controller prior to the simulation. An integrated simulation interface is working in the background.

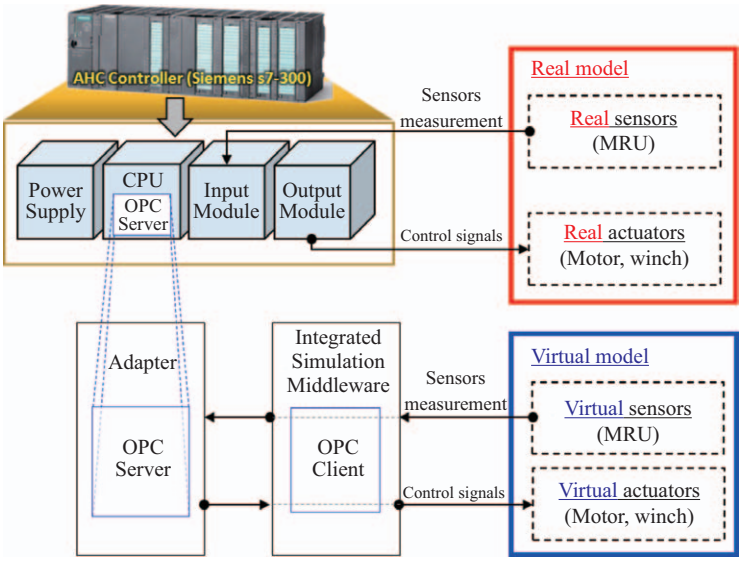

Fig. 15. The method of connecting the controller to the virtual model.

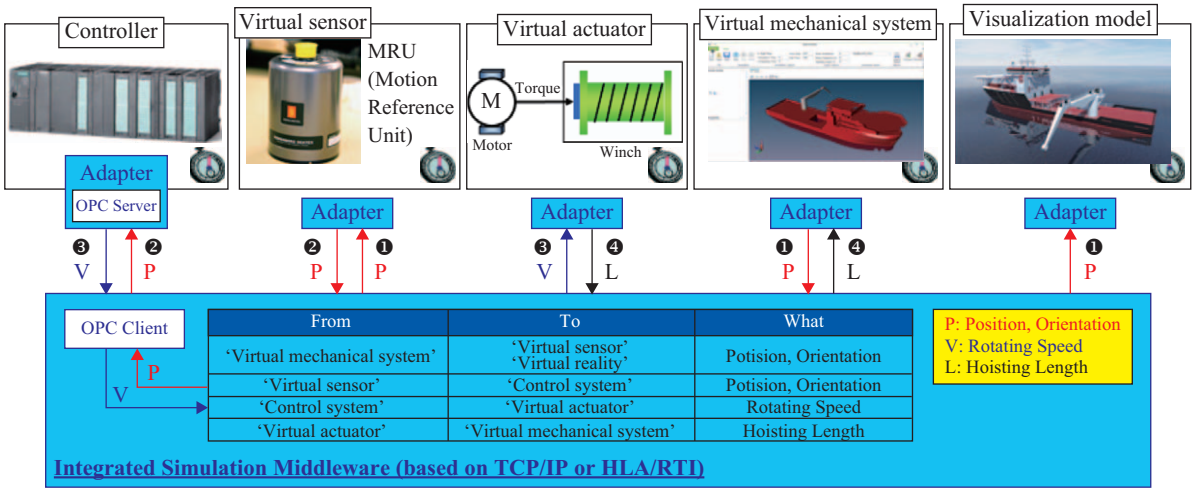

Fig. 16. Procedure for HILS of the AHC system with integrated simulation interface.

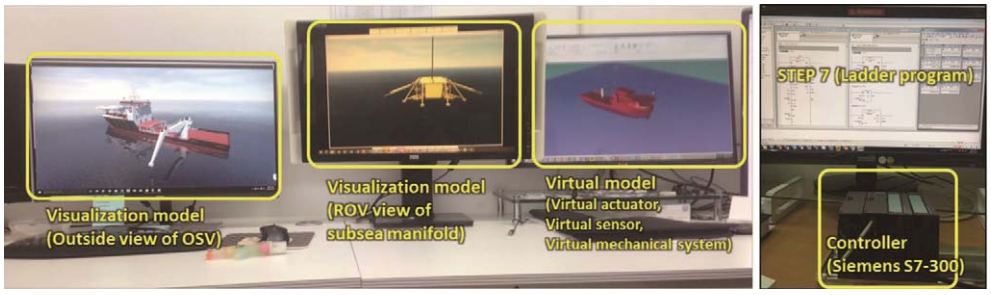

Fig. 17. Implementation of HILS in the AHC system.

IV. APPLICATIONS OF THE HILS ENVIRONMENT TO THE AHC SYSTEM

The performance analysis of the AHC system is conducted using the implemented components according to various wave conditions. Two kinds of control objectives are selected. One is to maintain the depth of the subsea manifold at a constant level. The other is to lower it to the seabed at a defined constant speed. Simulation results with control by AHC are compared with the simulation results without control.

Table 2. Wave conditions for maintaining the depth of the subsea manifold at a constant level.

Case	Type	Wave height (m)	Wave period (sec)	Wave direction (deg)	Target depth (m)
1-1	Regular wave	1.0	10	0	197.1
1-2				45	
1-3				90	
1-4	Irregular wave (JONSWAP)				

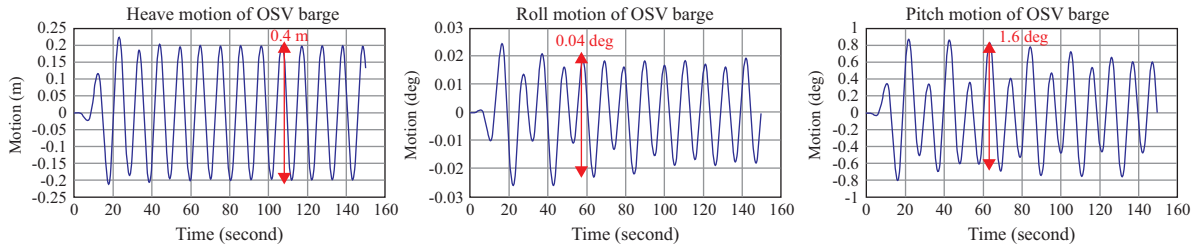

Fig. 18. Graphs of the heave, roll, and pitch motion of the OSV in Case 1-1.

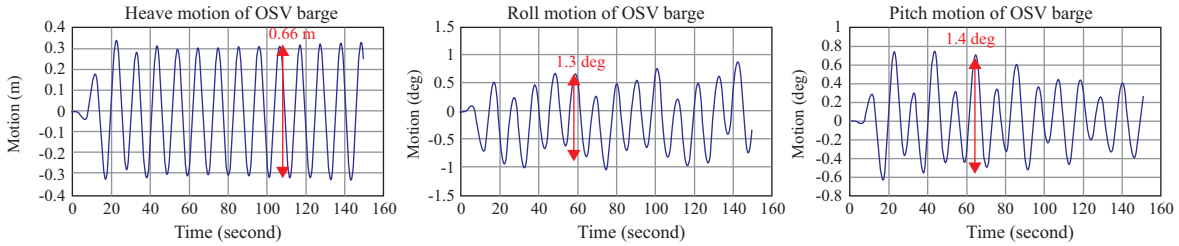

Fig. 19. Graphs of the heave, roll, pitch motion of the OSV in Case 1-2.

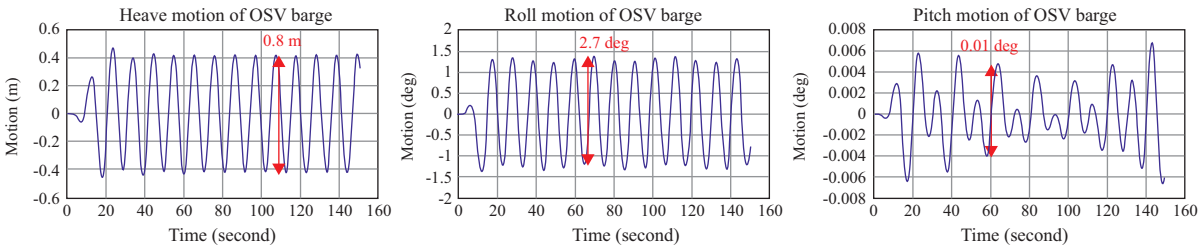

Fig. 20. Graphs of the heave, roll, pitch motion of the OSV in Case 1-3.

1. Maintaining the Depth of the Subsea Manifold at a Constant Level

Table 2 lists the simulation cases according to wave condition. Wave conditions, such as the wave amplitude, period, and direction, can induce different motions of the OSV. Here, we choose three cases from Case 1-1 to Case 1-3 for regular wave, and one case of Case 1-4 for irregular wave, to determine the effects of the wave direction. The extra peak enhancement factor (γ) of the JONSWAP spectrum in this study is 3.3.

Figs. 18-20 show graphs of the heave, roll, and pitch motion of the OSV in Cases 1-1, 1-2, and 1-3, respectively. According to the wave direction, the pitch motion is greater than the roll motion in Cases 1-1 and 1-2, whereas the roll motion is greater than the pitch motion in Case 1-3. Case 1-3 shows the greatest response among the three cases. In addition, the OSV crane uses the wire rope to maintain and lower the subsea manifold from the sea surface to the seabed. In other words, the motion of the OSV is affected not only by the wave force, but also by the spring force. As a result, the motion responses of the OSV show irregular phenomena, in spite of the regular wave.

Figs. 21-23 show the graphs of the heave motion of the subsea manifold in Cases 1-1, 1-2, and 1-3, respectively. The errors of the heave motion are reduced by approximately 98.3% from (0.43 to 0.007) m in Case 1-1, by 99.4% from (1.5 to 0.009) m in Case 1-2, and by 99.4% from (2.4 to 0.015) m in Case 1-3, respectively. Therefore, we can conclude that the performance of the AHC controller for maintaining the depth of the subsea

Table 3. Wave conditions for lowering the subsea manifold at a constant speed.

Case	Type	Significant wave height (m)	Peak wave period (sec)	Wave direction (deg)	Lowering speed (m/s)
2-1	Regular wave	1.0	10	0	0.1
2-2				45	
2-3				90	
2-4	Irregular wave (JONSWAP)				

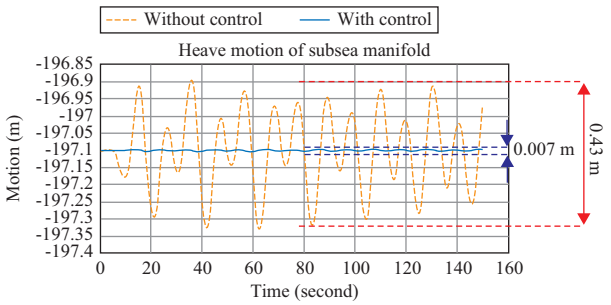

Fig. 21. Graph of the heave motion of the subsea manifold in Case 1-1.

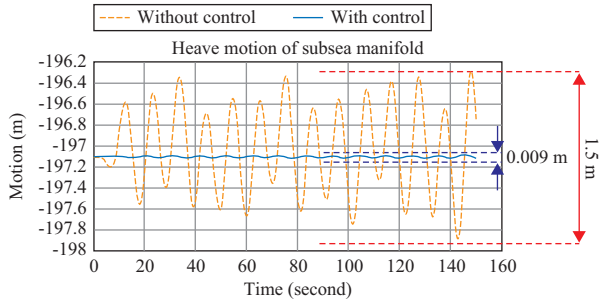

Fig. 22. Graph of the heave motion of the subsea manifold in Case 1-2.

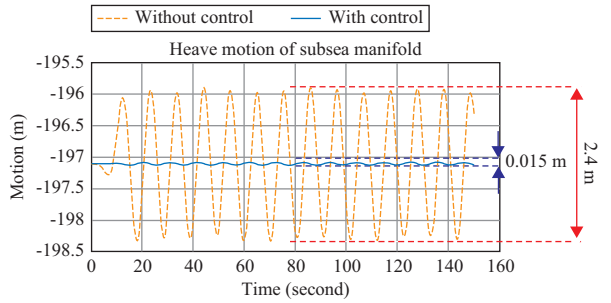

Fig. 23. Graph of the heave motion of the subsea manifold in Case 1-3.

manifold at a constant level has an error reduction ratio of more than 93%.

During the simulation, the motion of the subsea manifold was checked through the visualization model. Fig. 24 shows the visualization model of the subsea manifold in Case 1-3. When it is controlled, the subsea manifold maintains the depth at a constant level. On the other hand, when it is not controlled, it moves up and down across the centerline.

Meanwhile, the HILS in the case of an irregular wave type (JONSWAP spectrum) is conducted as Case 1-4. The significant wave height is 1.0 m, peak wave period is 10 seconds, and the other conditions are the same as in Case 1-3. This is performed for 10 minutes (600 seconds). Fig. 25 shows graphs of the heave and roll motion of the OSV.

Fig. 26 shows the graphs of the heave motion of the subsea manifold in Case 1-4. The heave motion with control is reduced by approximately 90.3% from (3.18 to 0.31) m in the irregular wave type.

2. Lowering the Subsea Manifold at a Constant Speed

Table 3 lists the same simulation cases that are applied in this application.

Figs. 27-30, respectively, show the lowering velocities of the subsea manifold of all cases. The errors of the lowering velocities are reduced by approximately 95.0% from (0.2 to 0.01) m/s in Case 2-1, by 95.6% from (0.68 to 0.03) m/s in Case 2-2, by 95.7% from (1.41 to 0.06) m/s in Case 2-3, and by 95.6% from (1.6 to 0.07) m/s in Case 2-4, respectively. Therefore, we can conclude that the performance of the AHC controller for lowering the subsea manifold at a constant speed has an error reduction ratio of more than 95%.

V. CONCLUSION AND FUTURE WORKS

The HILS of the AHC system is important to test the performance of the control algorithm in advance. To provide an elegant and efficient HILS environment, four components, such as the virtual model, controller, visualization model, and integrated simulation interface, were developed in this study. Finally, the system was applied to install a subsea manifold in regular and irregular waves for performance analysis of the AHC system. A comparative study between uncontrolled and controlled results of the AHC system was conducted. As a result, the performance of the AHC controller has an error reduction ratio of more than 98% for maintaining the depth of the subsea manifold at a constant level, and an error reduction ratio of more than 95% for lowering the subsea manifold at a constant speed. As a result, it can be seen that the performance of the AHC system can be effectively evaluated in the proposed HILS environment.

Future works will concentrate on making the HILS environment more realistic. For this, the virtual hydraulic motor and winch will be implemented based on real mechanisms. Furthermore, the added mass of the manifold in the seawater and the

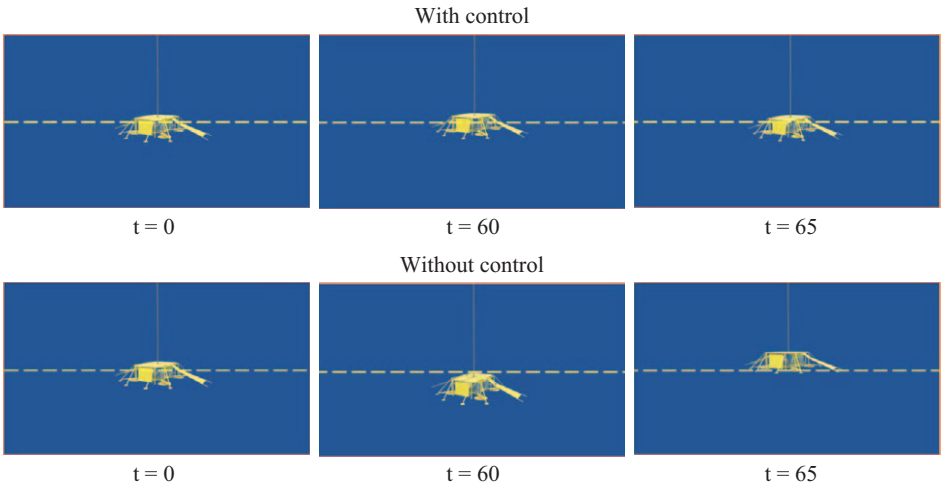

Fig. 24. Heave motion of the subsea manifold from the visualization model.

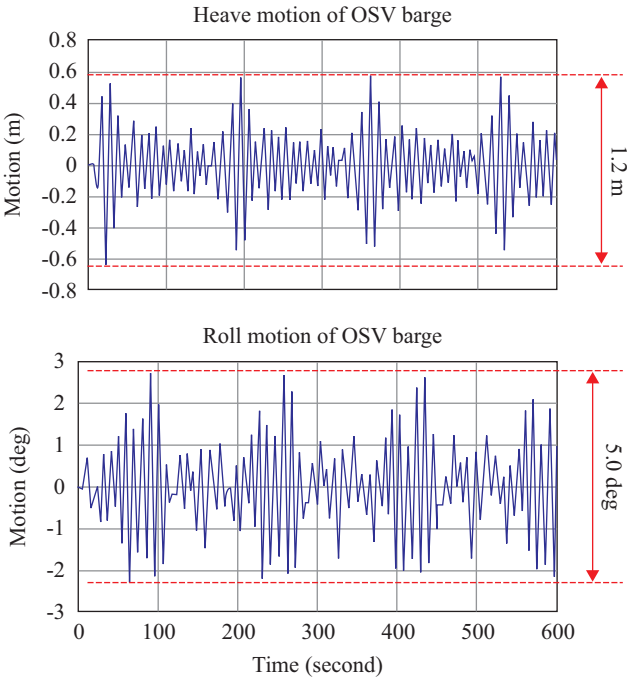

Fig. 25. Graphs of the heave and roll motion of the OSV in Case 1-4.

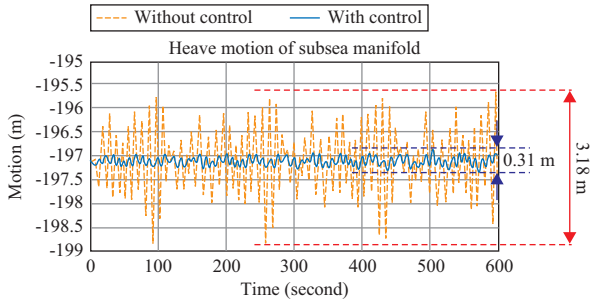

Fig. 26. Graph of the heave motion of the subsea manifold in Case 1-4.

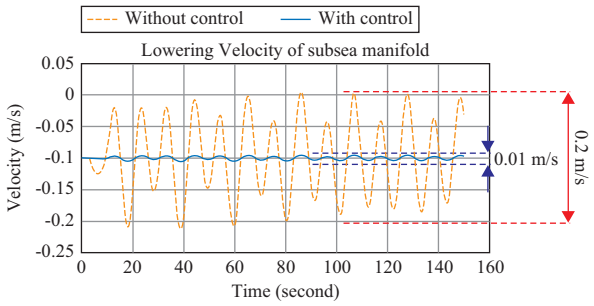

Fig. 27. Graph of the lowering velocity of the subsea manifold in Case 2-1.

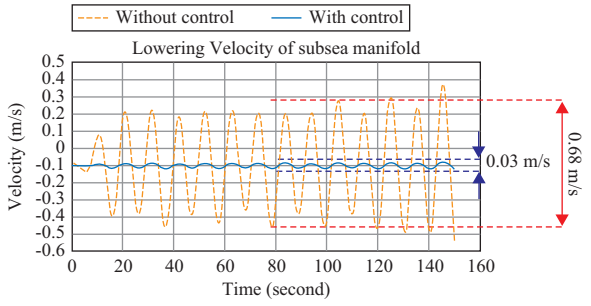

Fig. 28. Graph of the lowering velocity of the subsea manifold in Case 2-2.

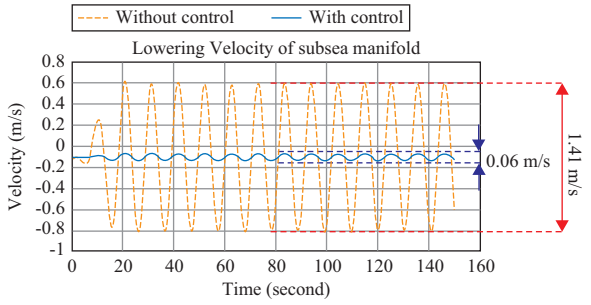

Fig. 29. Graph of the lowering velocity of the subsea manifold in Case 2-3.

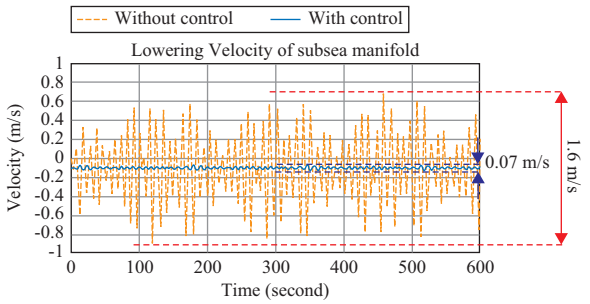

Fig. 30. Graph of the lowering velocity of the subsea manifold in Case 2-4.

external force on the wire rope must be considered more accurately in the future. Finally, we will perform experiments that include a motion platform, hydraulic motor, sensor, and controller, to simulate the real environment of the OSV crane. We will also compare the experimental results with the HILS result, to validate its effectiveness.

ACKNOWLEDGEMENTS

This work was partially supported by

(a) The National Research Foundation of Korea (NRF) grant funded by the Ministry of Education, Science and Technology (No. 2016R1A2B4016253),
(b) Research Institute of Marine Systems Engineering of Seoul National University, Republic of Korea, and
(c) Engineering Development Research Center (EDRC) funded by the Ministry of Trade, Industry & Energy (MOTIE), Republic of Korea.

REFERENCES

Aarseth, J., A. H. Lien, Ø. Bunes, Y. Chu and V. ÆsØy (2014). A hardware-in-the-loop simulator for offshore machinery control system testing. Proceedings of the 28th European Conference on Modelling and Simulation, Brescia, Italy.

Cha, J. H., M. I. Roh and K. Y. Lee (2010). Dynamic response simulation of a heavy cargo suspended by a floating crane based on multibody system dynamics. Ocean Engineering 37(14-15), 1273-1291.

Cummins, W. E. (1962). The impulse response function and ship motions. Schiffstechnik 9, 101-109.

DNV (2011). Modelling and analysis of marine operations, DNV-RP-H103.

DNV (2002). WADAM (Wave Analysis by Diffraction And Morison) theory, SESAM's user manual.

Fathy, H. K., Z. S. Filipi, J. Hagena and J. L. Stein (2006). Review of hardware-in-the-loop simulation and its prospects in the automotive area. Modeling and Simulation for Military Applications 6228.

Fowles, G. R. and G. L. Cassiday (2005). Analytical mechanics. Thomson Learning.

Journée, J. M. J. and W.W. Massie (2001). Offshore hydromechanics. Delft University of Technology, 6.40-6.41.

Ham, S. H., M. I. Roh, K. S. Kim, L. Zhao and S. Ha (2015a). Integrated simulation framework based on multibody dynamics, realistic visualization, and hardware for shipbuilding production and offshore installation. Proceedings of MARSIM 2015, Newcastle, UK, 1-7.

Ham, S. H., M. I. Roh, H. W. Lee and S. Ha (2015b). Multibody dynamic analysis of a heavy load suspended by a floating crane with constraint-based wire rope. Ocean Engineering 109, 145-160.

Ham, S. H., M. I. Roh and L. Zhao (2015c). Drillship simulation based on the integrated of motion analysis, virtual reality, and motion platform. Proceedings of the 29th Asian-Pacific Technical Exchange and Advisory Meeting on Marine Structures, Vladivostok, Russia, 198-202.

Hong, J. W., Ham, S. H., M. I. Roh and S. Ha (2015). Dynamic simulation of subsea equipment installation using an offshore support vessel based on flexible multibody system dynamics. Journal of Marine Science and Technology (Taiwan), 24, 807-821.

Hu, Q. and S. J. Liu (2009). A hardware-in-the-loop simulation system of heave compensation of deepsea mining. Proceedings of the International Society of Offshore and Polar Engineers (ISOPE), Chennai, India.

Isermann, R., J. Schaffnit and S. Sinsel (1999). Hardware-in-the-the-loop simulation for the design and testing of engine-control systems. Control Engineering Practice, 643-653.

Kaliappan, V. K., A. Budiyono and D. Min (2012). Hardware-In-the-loop simulation platform for the design, testing and validation of autonomous control system for unmanned underwater vehicle, Indian Journal of Geo-Marine Sciences, 41, 575-580.

Lew, A. J. (2003). Variational time integrators in computational solid mechanics. Ph.D. Thesis, California Institute of Technology, California, USA.

Marsden, J. E. and M. West (2001). Acta numerica. Cambridge University Press.

Merritt, H. E. (1967). Hydraulic control system, John Wiley & Sons, Inc, New York, 202-223.

Muraspahic, S., P. Gu and L. Farji (2012). Hardware-in-the-loop implementation for an active heave compensated drawworks. Central European Journal of Engineering, 2(2), 201-211.

Nabi, S., M. Balike, J. Allen and K. Rzemien (2004). An overview of hardware-in-loop-loop testing systems at Visteon. SAE World Congress, Detroit, Michigan.

OPC Foundation. 2016. What is OPC?, https://opcfoundation.org. (accessed on 30 Mar 2017)

Pedersen, T. and Ø. Smogeli (2013). Experience from hardware-in-the-loop testing of drilling control systems. SPE/IADC Drilling Conference, Amsterdam, The Netherlands.

Popovici, K. and P. J. Mosterman (2013). Real-time simulation technologies: Principles, methodologies, and applications. CRC Press, Boca Raton.

Schlager, M., W. Elmenreich and I. Wenzel (2006). Interface design for hardware-in-the-loop simulation. IEEE ISIE 2006, Montreal, Quebec, Canada.

Unity3D (2017). https://unity3d.com/. (accessed on 30 Mar 2017).